

***Pyrococcus horikoshii* TET2 Peptidase Assembling Process and Associated Functional Regulation**

Alexandre Appolaire¹, Eva Rosenbaum¹, M. Asunción Durá¹, Matteo Colombo¹, Vincent Marty¹,
Marjolaine Noirclerc Savoye¹, Anne Godfroy², Guy Schoehn¹, Eric Girard¹, Frank Gabel¹ and
Bruno Franzetti^{1,*}

¹ Institut de Biologie Structurale- CNRS, UMR5075, F-38027 / CEA, F-38054 / Université Joseph Fourier, France

² Ifremer, UMR6197, Laboratoire de Microbiologie des Environnements Extrêmes, France

*: Corresponding author : Bruno Franzetti, email address : franzetti@ibs.fr

Capsule

Background: TET aminopeptidases are 12 subunit complexes present in the three domains of life and are involved in important biological functions.

Results: The TET assembling process has been characterized. The oligomerization triggers TET activity toward large polypeptidic substrates.

Conclusion: The assembling of TET is a controlled process and regulates its activity in vivo.

Significance: This work provides a new example of peptidase regulation driven by self-oligomerization.

Abstract:

TET aminopeptidases are large polypeptide destruction machines present in prokaryotes and eukaryotes. Here, the rules governing their assembly into hollow 12-subunit tetrahedrons are addressed by using TET2 from *Pyrococcus horikoshii* (PhTET2) as a model. Point mutations allowed the capture of a stable, catalytically active precursor. Small angle X-ray scattering (SAXS) revealed that it is a dimer whose architecture in solution is identical to that determined by X-ray crystallography within the fully assembled TET particle. SAXS also showed that the reconstituted PhTET2 dodecameric particle displayed the same quaternary structure and thermal stability as the wild type complex. The PhTET2 assembly intermediates were characterized by analytical ultracentrifugation, native gel electrophoresis and electron microscopy. They revealed that PhTET2 assembling is a highly ordered process in which hexamers represent the main intermediate. Peptide degradation assays demonstrated that oligomerization triggers the activity of the TET enzyme toward large polypeptidic substrates. Fractionation experiments in *Pyrococcus* and *Halobacterium* cells revealed that, in vivo, the dimeric precursor co-exists together with assembled TET complexes. Taken together, our observations explain the biological significance of TET oligomerization and suggest the existence of a functional regulation of the dimer-dodecamer equilibrium in vivo.

Keywords: Aminopeptidase ; Archaea ; Biophysics ; Peptidases ; Proteasome ; Protein degradation ; Protein self-assembly ; Proteolytic enzymes ; Structural biology ; X-ray scattering

Efficient and controlled intracellular polypeptide breakdown is a primordial requirement that controls many cellular processes (1). Aminopeptidases constitute a group of enzymes of critical importance to intracellular regulatory networks. In addition to their key role in energy and amino acid metabolism, they contribute in a crucial manner to the protein degradation pathways by trimming the peptides released by ATP-dependent proteases such as the proteasome (2-5). Moreover, aminopeptidases remove post-translationally the N-terminal amino acid from precursor proteins thus directing their maturation and cellular localization, as well as controlling their half-lives (6). These enzymes equally assume important roles in specific biological processes involving peptide signalling, such as the production of the major histocompatibility complex ligands (7). Therefore, altered intracellular aminopeptidase activities have been associated with a variety of pathologies including aging, cataracts, cystic fibrosis, angiogenesis and cancers (5,8-10).

Numerous intracellular energy-independent peptidases co-exist in the cytosol but only a few of them share the capacity to self-assemble as large homo-multimeric complexes. These include bleomycin hydrolase, leucine aminopeptidase, DppA, TPPII, Tricorn protease, protease1, pab87 and the TET aminopeptidase (11-18). All these systems confine the peptidase activity to inner cavities, accessible exclusively to unfolded polypeptides. While most of them adopt a barrel-shaped architecture in which the active sites are lined up alongside a single central channel, the TET aminopeptidases form unique dodecameric edifices with a typical tetrahedral shape (18). The TET particle interior is accessible *via* the openings situated on each facet of the tetrahedron. The internal organization of TET peptidases revealed a highly self-compartmentalized system comprising a crossing network of four access channels extended by vast catalytic chambers in which three active sites are arranged in a circular fashion (19,20). This spatial arrangement is structurally different from all other self-compartmentalized protease complexes of known three-dimensional structure.

TET cytosolic enzymes belong to the M42 or M18 metallo-peptidase families in the clan MH according to the MEROPS classification system (21). The typical TET dodecahedral quaternary structure was initially described in Archaea (18,22,23). It was also

found in Bacteria (24) and, recently, the crystallographic structure of bovine and human tetrahedral aspartyl-aminopeptidases have revealed that the TET complexes are also present in eukaryotic cells (25,26). The quaternary structure of archaeal, bacterial and eukaryal TET assemblies is highly conserved. Their tertiary structures show that they all exhibit a two-domain architecture consisting of a catalytic and a dimerisation domain (19,24,25).

The high evolutionary conservation of TET peptidases in the three kingdoms of life suggests that they perform important biological functions. They were found to process polypeptides up to 27 aminoacids in length in the absence of ATP (18,27). Three different versions of TET complexes co-exist in the hyperthermophilic archaeon *Pyrococcus horikoshii*: PhTET1, PhTET2 and PhTET3. These complexes are built up in an identical fashion and have comparable dimensions. PhTET2 can be defined as a leucyl-aminopeptidase that displays a preference for neutral and aliphatic substrates, PhTET3 is a lysyl-aminopeptidase that hydrolyses preferentially basic residues and PhTET1 is a glutamyl-aminopeptidase that shows high specificity toward acidic residues (19,27,28). The comparison of the surface electrostatic potential features of the proteolytic chambers, and of the structures of the active sites pockets suggest a mechanism of substrate (N-ter aminoacid) discrimination based on the PhTETs internal surface electrostatic potential features (19,28).

The particular substrate specificities of the three TET variants in *P. horikoshii* suggest that they form a complementary set of enzymes (28). Because of their cooperative action, the archaeal TET peptidases can be designated as a "peptidasome" involved in the destruction of a vast variety of polypeptides. It has been suggested that, in peptide-fermenting organisms, the TET system plays an important role in the energy metabolism (19), or in the intracellular protein degradation by hydrolyzing the peptides produced by the proteasome endopeptidase activity (23). In addition, the TET peptidases could play more specific physiological roles as they can cleave physiologically relevant peptides. This hypothesis is supported by recent work on the eukaryotic tetrahedral aminopeptidase DNPEP that has been proposed to be a key player in the central nervous system,

in particular by regulating the ocular and renin system (25).

The TET enzymes are co-catalytic metallopeptidases, typically binding, by means of five amino acid ligands, two atoms of zinc or cobalt per monomer. The catalytic mechanism also implies a glutamate and an aspartate residue. Cobalt ions have a clear stimulatory effect on the amidolytic activity of PhTETs and the co-catalytic metals have been found to be important to maintain the PhTET oligomerization state (19,27-29). Unlike other self-compartmentalized peptidase, TETs are not processive enzymes that imply the detachment of the peptide moiety from the active site once the N-terminal residue has been cleaved (19,27,28,30). The mechanism of TET hydrolysis is extremely similar to the one of secreted monomeric aminopeptidase such as *Vibrio* aminopeptidase Ap1: it is the charge properties and the dimensions of the catalytic pocket of each monomer that triggers the specificity of the enzyme toward the N-terminal amino acid from the peptide chain (31). Thus, in the case of TET peptidases, the biological significance for oligomerization and active sites self-compartmentalization is not clear. To address this question, a site-directed mutagenesis strategy was used to slow down the natural oligomerization process of the PhTET2 complex. The structural properties of the purified PhTET2 dimer and of various oligomeric-forms intermediates were characterized by combining small angle X-ray scattering (SAXS), native gel electrophoresis, analytical ultracentrifugation (AUC) and electron microscopy. This allowed the dissection of the TET assembling pathway. The relationship between the aminopeptidase activity and its multimeric structure was also assessed by functional assays. Finally, density gradient fractionations and immunodetection experiments performed with *Halobacterium* and *Pyrococcus* cell extracts suggested the existence of a regulatory mechanism controlling the TET oligomerization state *in vivo*.

EXPERIMENTAL PROCEDURES

Pyrococcus horikoshii and *Halobacterium salinarum* cells cultivation – *P. horikoshii* was grown on SME YP medium, pH 7 (32) supplemented with PIPES (20 mM) and elemental sulfur (1 g/L). The cultivation was performed overnight at 90°C in 1 L serum vials containing 500 mL of medium under anaerobic conditions (N₂ gas phase). Cells were harvested by centrifugation and cell pellets were

immediately stored at room temperature in water/isopropanol (50/50 v/v) until utilisation. *H. salinarum* NRC1 was grown in hypersaline medium and processed as described (33). Cells were harvested at the end of mid-log phase.

PhTET2 cloning, expression and mutagenesis – Wild-type and mutant (R217S, R220S, F224S, H248S, I292A) PhTET2 genes were generated from synthetic DNA fragments optimized for codon usage in *Escherichia coli* and cloned in the overexpression plasmid pET41c by GeneCust Europe (<http://www.genecust.com>). The resulting constructs were transformed in the *E. coli* strain BL21 (DE3) for the recombinant expression of wild-type and mutated PhTET2 proteins as described in Durá et al. (2005) (27).

Protein purification – Total protein extracts from *E. coli* cells expressing the various recombinant PhTET2 proteins were prepared as described in Durá et al. (2005) (27). After heating at 85°C during 15 min to eliminate most mesophilic proteins from the *E. coli* host, the lysates were clarified by centrifugation at 17,400g for 1 h and the supernatant was loaded on a 6 mL Resource Q column (GE Healthcare) equilibrated in 100 mM NaCl, 20 mM Tris-HCl, pH 7.5. After washing with 3 column volumes, bound proteins were eluted with a linear salt gradient (0.1-0.35 M NaCl in 20 mM Tris-HCl, pH 7.5). In the case of the PhTET2 pentamutant, two well-separated elution peaks (called A and B) were observed. The fractions of each peak were combined and concentrated to 5 mg/ml using a centrifugal filter unit (Millipore) with a molecular mass cut-off of 10 kDa. For further purification and equilibrium shift assays, the proteins were loaded on a Superose 6 size exclusion column (GE healthcare) equilibrated in the desired buffer. To study salt (from 20 to 300 mM NaCl) and pH (7 to 9) effects, 50 mM HEPES and TAPS buffers were used. The purified proteins were kept at 4°C after the size exclusion step. Aliquots were analyzed on native gel electrophoresis as described below to observe the evolution of the equilibrium with time. Native gel electrophoresis in combination with analytical size exclusion chromatography experiments (see below) were systematically performed to determine optimal buffer conditions for AUC, SAXS and activity measurements, and to monitor the oligomerization state of the PhTET2 protein samples before and after experiments.

Native gel electrophoresis experiments – Native polyacrylamide gel electrophoresis (Native-PAGE) experiments were carried out to accurately identify the different PhTET2 subspecies generated upon incubation in different time and buffer conditions. Protein samples were mixed with one volume of loading buffer (20 mM Tris-HCl, 62.5% glycerol, pH 6.9) just before analysis. Polyacrylamide gels containing 8% acrylamide-bis-acrylamide, 20 mM NaCl, 50 mM Tris-HCl, pH 8.8, were run at 4°C for 90 min in a Tris-glycine buffer (25 mM Tris-HCl, 192 mM glycine, pH 7.5). The protein bands were visualized by Coomassie Brilliant Blue staining. The ratios between the different PhTET2 species that were detected on native gels electrophoresis were found to be in excellent agreement with those determined on the same samples and in the same buffer by size exclusion experiments on a Superose 6 column.

Analytical Ultracentrifugation (AUC) – Sedimentation velocity experiments were performed at 20°C on different samples of the purified mutated PhTET2 protein with an Optima XL-1® analytical ultracentrifuge (Beckman) at 42,000 rpm with a 50-Ti eight-hole rotor (Beckman). The analyzed samples were prepared in 50 mM HEPES, 300 mM NaCl, pH 7.5 buffer at a protein concentration of 0.4 mg/mL as described above. Two-channel centrepieces with an optical path of 12 mm were used and all experiments were performed using sapphire windows. Scans were recorded at 280 nm with radial spacing of 0.005 cm. The program Sednterp was used to estimate the partial specific volume from amino acid composition as well as the density ρ and viscosity η (jphilo.mailway.com). Data were analysed with the program Sedfit (34) using a continuous c(s) distribution model.

Small angle X-ray scattering (SAXS) – All experiments were performed on the beamline BM16 at the European Synchrotron Radiation Facility (ESRF) (Grenoble, France). Scattering curves of the samples were measured at 80°C. The scattering patterns were corrected for background scattering and the geometry of the experimental arrangement. Three samples were measured: the mutated dodecamer of PhTET2 (PhTET2-12s), purified to homogeneity just before the experiment and concentrated up to 2.9 mg/mL in 50 mM HEPES, 20 mM NaCl, pH 7.5; the mutated dimer of PhTET2 (PhTET2-2s), purified to homogeneity just before the experiment and concentrated up to 3 mg/mL in

50 mM TAPS, 20 mM NaCl, pH 9; and the wild type dodecamer of PhTET2 (PhTET2 WT), purified to homogeneity just before the experiment, concentrated up to 3.5 mg/mL in 50 mM HEPES, 20 mM NaCl, pH 7.5. The *ab initio* envelope was generated using the program GASBOR (35). Fifteen models were averaged and filtered with the help of the program DAMAVER (36). The resulting bead model was transformed into a volumetric map using the program pdb2vol from the Situs program package (37) and the crystallographic model was placed into this map by rigid body docking with the program Colores (38). The theoretical SAXS curves were calculated with the program CRY SOL (39) in default mode. The missing fragments were modelled (internal loop, 120-132 and the N-ter 1-5) in the PhTET2 12s structure and were added using PyMOL Molecular Graphics System, Version 1.5.0.4 Schrödinger, LLC. and Coot (40)

Electron Microscopy – The dimeric fraction of PhTET2 was incubated in HEPES 50mM, 150 mM NaCl, pH = 7.5 after the size exclusion column step of the purification. The reoligomerization was followed by native gels and gel filtration. The intermediate fractions were isolated from the dimer and dodecamer of PhTET2 and pooled in a ‘low molecular weight intermediate’ sample and a ‘high molecular weight intermediate’ sample.

4 μ L of the PhTET2 sample (~0.1 mg/ml) were loaded between the mica-carbon interface as described in Franzetti et al. (2002) (18). The sample was stained using 2% sodium silicotungstate pH 7.5 and air-dried. Images were taken under low-dose conditions in a CM12 Philips electron microscope working at 120 kV and with a nominal magnification of 40,000 using an Orius SC1000 CCD camera.

The different pdb files generated by molecular modelisation were loaded into SPIDER (41) and filtered to 20 Å 3D structures. Those structures were reprojected in all directions with a 10 degrees spacing and the reprojections were compared by cross correlation with raw negative staining images selected from the CCD frames. For each structure, the best cross-correlating images were carefully examined by eyes. The best matching and unambiguous images and the corresponding 3D model orientation were selected and included in figure 5. Special care were taken to include only model specific representative views (reprojections and views that are not overlapping with other model

reprojection views).

Enzyme activity assays – Activity on mono-acyl-pNA peptides: PhTET2 hydrolytic activity on different synthetic chromogenic compounds was determined using aminoacyl-pNAs as described (27). Four replicates and four enzyme blanks were assayed for each experimental point. Leu-pNA was used for half-life calculations as described (27). Half-lives were calculated from a first-order exponential decay fit to the experimental points.

Activity on polypeptides: PhTET2 hydrolytic activity on synthetic peptides was determined through a procedure inspired from Frottin *et al.*, (2006) (42). Different commercial polypeptides containing a poorly hydrolyzable residue in P₁ position were assayed. Reactions were initiated by addition of the enzyme (0.1 mg/mL) to 140 μ L of a pre-warmed reaction mixture containing 0.1 mg/mL *o*-dianisidine (Sigma), 3 units of horseradish peroxidase (Sigma), 0.5 units of L-amino-acid oxidase (Sigma), and 0.1-6 mM peptide in 50 mM PIPES, 150 mM KCl, 1 mM CoSO₄, pH 7.5. The hydrolytic activity was assayed by monitoring the absorbance of oxidised *o*-dianisidine at 440 nm, coupling the PhTET2 activity to both L-amino-acid oxidase and peroxidase activity, according to the reaction sequence described by Frottin *et al.*, (2006) (42). Assays were performed in 1mm-thick quartz cuvettes. Absorbance evolution was measured using a Beckman spectrophotometer DU 7400 equipped with a thermostat and a 6-position sample changer. The hydrolytic activity of PhTET2 was measured at 40 °C. To calculate the concentration of oxidized *o*-dianisidine in solution, the molar extinction coefficient used was $\epsilon=10,580 \text{ M}^{-1}\text{cm}^{-1}$. Catalytic constants K_m and k_{cat} were estimated using the enzymology tools of SigmaPlot version 11.0 from Systat Software, Inc. (www.sigmaplot.com). For a same mass concentration, the molecular concentration of dimer is six times higher than the one of the dodecamer. The difference between the mass and the molar concentrations has been taken into account during the estimation of the kinetic parameters. Four replicates and four enzyme blanks were assayed for each experimental point.

Sucrose density gradient fractionations and protein immunodetection experiments – P. horikoshii cell pellets (0.2 g) were suspended in 1 mL of lysis buffer (150 mM KCl, 50 mM Tris-HCl, 40 mM MgCl₂, DNase 1 grade I (Roche, 0.05 mg/mL), pH 7.6). The disruption of the cells was achieved by sonication (10 pulses of 20

sec at medium power with a Brandson Sonifier 50). The crude extracts were clarified by centrifugation at 30,000 g for 30 min at 4°C (Ultracentrifuge Beckmann Optima-TL 100) and 250 μ L of the post-membrane protein cytoplasmic extracts (S30) were gently loaded on 5-25% continuous sucrose density gradients made in 10 mL Beckman ultra-clear centrifuge tubes. The sucrose density gradients were centrifuged at 210,000 g during 20 hours (Beckmann L-80 ultracentrifuge, SW-41 Ti rotor). *H. salinarum* cellular extracts and sucrose density gradient experiments (5-20%) were performed in native hypersaline conditions as described in Chamieh *et al.* (2008) (33).

Purified dodecameric and dimeric forms of the mutated PhTET2 protein were run simultaneously on separate tubes. The gradients were fractionated into 750 μ L aliquots. In *P. horikoshii* S30 fractionation experiments, the proteins were precipitated from the fractions during 30 min at -20°C with trichloroacetic acid (15% final concentration). After centrifugation at 16,000 g during 30 min at 4°C, the pellets were washed with glacial acetone and the samples were immediately centrifuged for 15 min at 16,000 g at 4°C. The pellets were air-dried for 10 min before resuspension in ice cold 20 mM Tris-Base. One volume of SDS-PAGE loading buffer (50 mM Tris-HCl, 8 M urea, 2 M thiourea, 100 mM DTT, 3% SDS, 0.1% bromophenol blue, 10% glycerol, pH 6.8) was then added to the samples. These were heated at 95°C for 5 min and their proteins separated by SDS-PAGE using 12% gels. Staining was done with Coomassie Brilliant Blue or the proteins were transferred onto Hybond-P PVDF-membranes and immunoreactive bands were visualized by chemiluminescence as detailed by the supplier (ECL detection kit; GE Healthcare). The signal was detected using a Kodak Image station 4000mm. Specific PhTET2 antibodies were raised against the following synthetic peptides chosen in the protein primary sequence: DERDVDATVELMTKALENIHELKI. The anti HsTET antibodies were raised against two peptides: TRGSQVRIETDDGPV and AHAGDRDSFGVSV. The anti-sera were used at 1/2.500 and 1/10000 dilution for PhTET2 and HsTET, respectively. The experiment has repeated at least three times with Ph and Hs cell batches from different cultures.

RESULTS

Purification and structural characterization of a dimeric PhTET2 precursor

– For this study the PhTET2 complex from *P. horikoshii* has been chosen. The protein exhibits high thermal stability and, compared to other types of TET complexes, it possesses broader substrate specificity. Additionally, it can be purified in large amounts without adding tags that may create artifacts when studying the oligomerization process. When recombinant PhTET2 proteins are expressed in *Escherichia coli*, only the dodecameric complex was detected in the soluble post heat-shock fractions. Moreover, once assembled, the TET particles are extremely robust *in vitro* and can only be broken down into smaller oligomeric forms by using extreme pH conditions and EDTA treatments (29). These harsh physico-chemical treatments do not allow the functional characterization of the low molecular weight species; moreover the process is only partially reversible and generates aggregates. We have therefore used a site-directed mutagenesis approach in order to study the TET assembling process and the influence of the enzyme's oligomerization state on its catalytic and thermal stability properties. The examination of the subunit interfaces in PhTET1, PhTET2 and PhTET3 according to their crystallographic structures, as well as the structural study of a 24 subunit PhTET1 complex, suggested that the dimer is the building block of the PhTET edifices (19,28). Point mutations were therefore designed to weaken the interactions at the interfaces between the dimers within the dodecamer. Some of them were changed to serine instead of alanine to completely eliminate the possible formation of any hydrophobic interaction of the side-chain methyl group of the alanine, and also to make the interface more polar. However, neither single nor double mutations could appreciably alter the rate of TET dodecamer formation in the post heat-shocked supernatant of the transformed *E. coli* cells, and only after a combination of five mutations (R217S, R220S, F224S, H248S and I292A) a significant slowdown of the oligomerization process was achieved. The 5 mutations are mostly located in the prominent inter-subunit interaction regions located at the apices of the tetrahedron on residues participating in hydrophobic clusters, but also in polar contacts (for details see Suppl. Fig. 1).

When the post heatshock protein extracts of *E. coli* cells expressing the PhTET2 pentamutant were resolved on a Resource Q ion

exchange column, two well-separated elution peaks were obtained while the expression of the wild-type PhTET2 protein produces only one peak. The corresponding fractions were pooled (Pool A and Pool B). Native gel electrophoresis analysis revealed that the pool A contained a homogeneous population of low molecular weight oligomers, while the pool B contained predominantly large oligomers that migrated as the wild type TET dodecamer (Fig. 1A). The two oligomeric forms of the mutated PhTET2 proteins were further purified by size exclusion chromatography (Fig. 1B). The A pool contained PhTET2 oligomers with an apparent molecular mass <100 kDa, while the B pool principally contained a large complex. According to the molecular weight calibration of the size exclusion column and to negative staining electron microscopy images, the low molecular weight form would correspond to a free TET dimer (78 kDa), while the larger complex was a dodecamer (468 kDa), as clearly shown by the negative staining electron microscopy pictures that revealed its tetrahedral shape, identical to that of the wild-type TET (Fig 1B).

TET low molecular weight complexes co-exist with the assembled dodecamers in vivo— In order to gain insight into the oligomerization state of the PhTET2 aminopeptidase complex *in vivo*, post-membrane protein cytoplasmic extracts (S30) from *P. horikoshii* cells were resolved through continuous sucrose density gradients. Fractions were collected and the PhTET2 proteins were immuno-detected in each fraction by using a specific antibody (Fig. 2A). Two major populations of native PhTET2 proteins complexes were found to accumulate in the cellular extracts: a high and a low-molecular weight species. To assess their respective oligomerization state, purified pentamutant PhTET2 dodecamer and dimers were analyzed on separate gradients, in the same experimental conditions. The dimeric form was obtained from a PhTET2 mutant that is described in this article. It showed that the high molecular weight complex detected in *P. horikoshii* sedimented as the purified recombinant dodecamer, while the low molecular weight species would correspond to a PhTET2 dimer (Fig. 2A). This indicates that the 5 mutations introduced in the PhTET2 interfaces indeed lead to the stabilization of the low molecular weight form observed *in vivo* (Fig. 2A). This result is interesting since, when wild type PhTET2 proteins are expressed in *E. coli*, only the dodecameric complex is detected

in the soluble post heat-shock extract.

In order to confirm the presence of unassembled TET complexes in the cytosol of archaeobacteria, we performed similar cell fractionation and immunodetection experiments in *Halobacterium salinarum* (Hs), an extreme halophilic organism that accumulates multimolar salt concentration in its cytosol (43). For this reason all experiments on Hs samples, including sucrose gradients sedimentation, were performed in physiological hypersaline conditions (3.4M KCl) as described in Chamieh et al 2008 (33). The results are shown in figure 2B. As in the *P. horikoshii* extracts, a low molecular weight species of TET with an apparent molecular mass <100 kDa is present together with the fully assembled TET particle. We concluded therefore that, *in vivo*, a significant population of low molecular weight TET complexes, presumably dimers, co-exists with the assembled TET dodecamers.

Quaternary structure and thermal stability comparisons between the wild type and the pentamutant PhTET2 dodecamers – The presence of low molecular weight forms of the TET complex *in vivo* prompted us to study their structural and biochemical properties as well as the TET assembling mechanism. The structural and biophysical properties of the mutant dodecameric particle were therefore studied to determine the potential effects of the mutations on its final quaternary edifice. To this end, small angle X-ray scattering (SAXS) curves were recorded on the mutant dodecamer in solution and compared to those of the PhTET2 wild-type protein. Both sets superposed nicely with the SAXS data from the wild type TET, even when the experiments were performed at 80°C, thus showing that the quaternary structure of the mutant is identical and equally stable as the one of the wild-type TET at the extreme physiological temperatures in which *P. horikoshii* thrives (Fig. 3). The agreement of the theoretical SAXS curve (calculated with CRY SOL) with the experimental data is good, in particular when the missing loop and the N-ter (not visible by X-ray crystallography) were modelled. The remaining discrepancy at the side-minima could be explained by the conformational flexibility of these two fragments which produces a smearing of side-minima in SAXS curves of globular objects (see, e.g. Glatter in Lindner and Zemb, 2002) (44).

These experiments show that Wt and mutant PhTET2 particles are therefore extremely

stable once they are formed and the deleted interactions located at the dimer-dimer interfaces do not contribute to the stability of the dodecameric structure at high temperatures.

SAXS structure of the free TET dimer – Since the dimer is the basic building unit in the dodecameric TET particle (19), it is important to characterize its structure further in order to understand the mechanisms underlying the TET oligomerization process and to address the question of the physiological significance of unassembled dimers *in vivo*. While crystallographic studies of the mutated free dimer are not possible due to its self-assembling properties, its oligomerization kinetics are slow enough to allow SAXS studies on monodisperse dimeric samples, even at 80°C. The SAXS experimental curve obtained from the free dimer superposed nicely, up to a scattering vector $Q=0.15 \text{ \AA}^{-1}$, with that calculated (with CRY SOL) from the crystallographic dimer structure within the wild-type dodecameric assembly (PDB entry 1Y0R) (Fig. 4A), in particular when the missing internal loop and the N-ter were added. The minor mismatch around $Q=0.20 \text{ \AA}^{-1}$ can probably be explained by a conformational flexibility of the loop and N-ter as in the case of the dodecameric structure in Figure 3. Moreover, the crystallographic structure of the dimer can be embedded very nicely into the *ab initio* envelope (Fig. 4B). A dimer of dimers (tetrameric V-shaped structure) and a trimer of dimers (hexameric triangular-shaped structure) did not fit the experimental SAXS data. We therefore conclude that the structure of the free dimer in solution is very similar to that of the wild-type dimer within the dodecamer. Thus, no major conformational changes of the TET dimer precursor seem to be necessary to constitute the 12-subunit tetrahedral particle.

Biophysical characterization of the PhTET2 oligomerization process – The results described above showed that the mutated PhTET2 is fully able to self assemble into a *bona fide* TET machine that maintains the same quaternary structure and thermal stability properties as the wild type TET. Consequently, the pentamutant represents a model to study the oligomerization process. In order to identify the parameters controlling the equilibrium between the different oligomeric forms, samples were incubated in different buffers after the size exclusion purification step (see “Materials and Methods”). At physiological pH, the formation of dodecamers from the dimer can be stimulated

by a slight increase in salt concentration while the dimer is stabilized at high pH. Native gel electrophoresis analysis performed at different times after incubation of the purified dimer revealed well-defined bands corresponding to intermediate oligomeric states between the dimer and the dodecamer (Fig. 5A). The different oligomeric species were characterized by analytical ultra-centrifugation (AUC) (Fig. 5B and C). Native gels electrophoresis and AUC analyses showed the same number of intermediates. Sedimentation profiles displayed multiple, different, peaks at 4.70, 6.78, 9.29, 11.91 and 15.75 S, indicating the presence of five species in the sample. The same number of species was observed on native gels electrophoresis. Using the Svedberg equation (45) we calculated theoretical sedimentation coefficients for dimeric and dodecameric PhTET2 as well as for putative intermediates (Fig. 5C). Accordingly the peaks were assigned to, respectively, dimer, tetramer, hexamer, octamer and dodecamer of PhTET2.

The native gel analysis of the different assembling intermediates revealed that the tetrameric form is the first one to be detected. Interestingly, the accumulation of the octamer precedes the apparition of the hexamer, we could not detect decamer and no intermediate forms with odd subunit numbers were identified (Fig. 5C). These experiments demonstrated that the TET oligomerization process is a non-random, stepwise process.

Electron microscopy and structural modelling of the different PhTET2 intermediates – The PhTET2 assembling intermediates identified by AUC and native gels were separated from the dimer precursors and from the final TET dodecamer by using gel filtration chromatography. The column fractions were analyzed by electron microscopy. Three types of well-structured edifices were identified in the samples: a tricorn shaped complex, an open chain, and a complex with a four-fold symmetry. The sizes of these complexes were consistent with the hexameric and octameric intermediates complexes. Smaller, less structured, species that would correspond to the tetramers could also be seen. To propose structural models for the octameric and hexameric TET assembling intermediates we generated the dimeric building blocks from the crystal structures of PhTET2 (PDB code: 1Y0R). By using the oligomerization interfaces that were

identified in the PhTET dodecamers it was possible to generate a tricorn complex made of 3 dimers (Fig. 6). Alternatively, 3 dimers can also assemble as an open chain with a Z shape (Fig. 6). These two assemblies can be recognized in the dodecamer.

The existence of complexes with a four-fold symmetry cannot be modeled from the 12-subunit dodecamer structure. We used instead the 24-subunit structure that has been described for PhTET1 (19). Indeed, this tetraicosameric edifice is not fashioned through the assembly of two dodecamers but the octamer is one vertex of the 24-mer assembly. The octamer uses different inter-subunit contacts than the dodecamer. In particular the interface with the five proposed mutations is not involved in the octamer. As the rmsd deviation between the PhTET1 (PDB code 2CF4) and PhTET2 dimers were 5.1 Å over 660 C α atoms, we used the PhTET2 dimer for modeling octamer. Accordingly, we extracted an octameric structure from the PhTET1 24-subunits one and superimposed the PhTET2 dimer structure to produce a PhTET2 octamer model. The structures corresponding to the octameric and hexameric models are presented in figure 6. Low-resolution envelopes were generated from the corresponding coordinates files for back projection using Spider (41). The experimental electron microscopy images were compared with the different views of the complexes (see “Materials and Methods”) (Fig. 6). As a control, the same work was performed with the final TET particle in order to clearly distinguish the differences between the shapes and dimensions of the tricorn and the TET dodecamer respectively. Model specific images could be found for each of the complexes’ orientations. The shapes and dimensions of the single particles identified by electron microscopy are well consistent with those arising from the modelling, the AUC and the native gel experiments. These results indicate that the proposed octameric and hexameric (tricorn and open chain) structures correspond to the octameric and hexameric intermediates that were identified in the PhTET2 assembling pathway.

The octameric square complex is build upon different interfaces to the two hexameric forms and the final TET dodecamer. The same interactions can be used to generate the tetramer intermediates. The five mutations that were

designed to slow down the TET assembling process do not impact the alternative contact area present in the tetramers and octamers. Accordingly, the mutations favor the accumulation of tetramers and octamers while the efficient formation of hexamers is delayed. This explains why the tetramers and octamers preceded the apparition of the hexamers during the assembling process of the PhTET2 pentamutant. It is worthy to note that the formation of the TET dodecameric apices that possess a 3-fold symmetry cannot arise directly from the tetramers or octamers structures. This indicates that the tetramers and octamers are the products of an alternative pathway induced by the mutations.

Oligomerization triggers PhTET2 activity toward large polypeptidic substrates – In order to study the role of the oligomerization with respect to the functional state of the aminopeptidase, the hydrolytic activities of the mutated PhTET2 dimer and dodecamer were first measured by using short chromogenic aminoacyl compounds as described by Durá *et al.* (2005) (27). These experiments were performed on a time scale of several minutes after the size exclusion purification step. As a control, aliquots were taken from the reaction mixture and analyzed by size exclusion chromatography and native gel electrophoresis to be sure that the dimers and dodecamers had not formed other multimers during the experiments. The rate of Leu-pNA cleavage performed by the enzyme dimeric forms and its comparison with the one of the mutant dodecamer revealed that, at 40 and 80°C, the activity of the two types of oligomers is nearly identical. The K_m and k_{cat} values were found to be very similar for the two types of TET assemblies (Table I). This study shows that the dimeric form of TET is active and that the assembling of the protein into a 12-subunit tetrahedral superstructure does not modify significantly its amidolytic activity toward small substrates.

The aminopeptidase capability of the dimer raised the question of the biological significance of the TET supramolecular complex. We previously showed that TET peptidases display a significant hydrolytic activity toward the N-terminal residue of oligopeptides up to 27 amino acids in size (27). When the activities of the mutant PhTET2 dodecamer and dimer were tested against longer peptides such as AAA-pNA

and AAAA-pNA, a significant lag phase was observed in the case of the dimer. This suggests that the size of the peptide is an important parameter for substrate hydrolysis when comparing dimers to the fully assembled TET complex. To obtain kinetic constants from long polypeptides (about 10 amino acids in length), substrates that contained a favorable N-terminal residue and an unfavorable residue in position P'₁ were used. In this manner, the quantity of released amino acids reflects only the hydrolysis of the first residue, allowing the calculation of kinetic parameters. The enzymatic assay employed was inspired from that developed by Frotin *et al.* (2006) (42). Again, the oligomeric state of the TET aminopeptidase was checked before and after the experiments. Two oligopeptides were tested: Met-Lys-Bradykinin (MKRPPGFSPFR) (Fig. 7) and MBL peptide 175-185 (VDLTGNRLTY) (data not shown). In both cases, we observed that the dodecamer was more active than the dimer and, unlike for the short peptide experiment, an important difference in the reaction speed between the two PhTET2 oligomeric forms was observed. We measured the K_m and k_{cat} values of the dimer and dodecamer of the PhTET2 pentamutant for the Met-Lys-Bradykinin peptide (Table I). The K_m of the dimer and the dodecamer were found to be identical. However, the k_{cat} value of the dimer was significantly lower than the one of the dodecamer. Thus, the TET reaction efficiency toward long peptides is compromised when the enzyme is not assembled as a dodecameric complex. These results demonstrate that oligomerization allows the TET peptidase to better process long polypeptides. Therefore, the dimeric and dodecameric forms that we detected *in vivo* in two archaeal strains (Fig. 2A and B) may perform different physiological roles.

The PhTET2 dimer is stable under high temperature conditions – The TET dimer represents the minimal assembling unit in the TET oligomerisation pathway (19), and this observation raises the question of the dimer stability under the extreme temperature conditions that prevail in the natural environment in which *Pyrococcus* cells thrive. The SAXS experiments described in this paper have demonstrated that, *in vitro*, the dimer population does not show any sign of structure alteration at 80°C, within one hour (Fig. 4A). In order to further explore the thermal stability of the TET dimer, the residual aminopeptidase activity after different times of incubation at 80°C was

measured as described in (27). Leu pNA was used as a substrate. Aliquots were taken at different incubation times. Native gel and gel filtration experiments were performed to verify that no evolution of the protein oligomeric state had occurred during the incubation time. The calculated half-life values of the mutant dimeric and dodecameric forms were found to be the same as those of the wild type PhTET2 determined earlier (about 10 hours) (27). These findings indicated that the extreme thermal stabilization of the TET particles is not achieved through dodecamerization and that, under extreme physiological temperatures, free TET dimers which are catalytically active against small peptides, could be accumulated in the *Pyrococcus* cells as precursors of the TET complex.

DISCUSSION

A key question regarding self-compartmentalized peptidase complexes are the mechanisms by which such well-organized edifices assemble. In this paper, a site-directed mutagenesis strategy has been used to slow down the self-assembling process of TET, a large dodecameric aminopeptidase present in the three domains of life. The disruption of stabilizing interactions located in the interfaces area between the subunits at the apices of the tetrahedron had a significant effect on the kinetics of the TET assembling process. By this way, a stable dimeric species could be purified which was fully able to self-assemble into active dodecamers. Small angle X-ray scattering (SAXS) studies showed that the dodecameric particle obtained from the mutant dimer displayed the same stability and quaternary structure as the wild-type TET complex, even under extreme temperatures.

Native gel electrophoresis, AUC and electron microscopy analyses proved that the mutant PhTET2 oligomerization does not proceed by an incremental addition of dimers but involves well-defined intermediate species that are generated with time from the PhTET2 dimer precursor. While tetramers and octamers were detected at the beginning of the oligomerization process, they are the products of an alternative pathway induced by the mutations. Based on SAXS analysis of the free PhTET2 dimer, electron microscopy study and structural modeling from existing crystallographic structures of the PhTETs (19,23) we propose that the natural pathway involves two hexameric intermediates: a

tricorn and an open (Z-form) chain complex. Indeed, the tricorn represents a stable oligomeric form in solution. However, the Z-form is able to self-associate, leading to the extended interaction zone involving the catalytic domains of three subunits present in the highly stable biological dodecamers. Consequently, we propose that the open and closed hexamers are in equilibrium and represent the intermediates in the PhTET2 dodecamer assembling process (Fig. 8). The oligomerization interface that is present in the PhTET2 hexamers and dodecamers is well conserved in the three PhTETs (data not shown). This suggests that the oligomerization process and the associated functional activation that we described for PhTET2 may also be valid for PhTET1 and PhTET3.

Self-compartmentalization is a hallmark of cytosolic peptidases that degrade peptides in an unspecific manner (46). In the proteasomes, tricorn protease, and bleomycin hydrolase the sequestration of the catalytic sites from the bulk environment into chambers represents a peptide filtering system that is necessary to prevent unwanted damage on folded polypeptides within the cytosol (47-49). Oligomerization has also been shown to control different aspects of the peptidases functions. In the 20S proteasome and its bacterial homologue ClpP, the priming of the peptidase enzymatic activity is coupled with subunit association (50). In ATP-independent peptidases, such as Protease 1 and Pab87, the active sites are formed at the subunit junctions (16,17). In TPPII, a giant aminopeptidase found in eukaryotes, the activity increases in a non-linear fashion with the oligomerization rate (11) and, in the case of bovine lens leucyl aminopeptidase, it has been suggested that the activity depends on the stabilization of each monomer catalytic site by the structure of the oligomer (51). On the contrary, in α -1 tryptase or kallikrein-related peptidases (KLKs) self-oligomerization provides an inhibition of the enzyme activity (52,53). With respect to these findings it was surprising to find out that the dimeric form of the TET complex still carries out the same catalytic activity on small peptides as the 12-subunit complex. This indicates that, in the TET dimers, the catalytic sites and pockets are already positioned in proteolytically active conformations. The SAXS structure of the free dimer is consistent with these findings, since it shows that the relative positions of the two monomers of each dimer within the tetrahedral

complex are already imposed by the interactions between dimerisation domains. In the case of this small peptide, the calculated K_m are similar, meaning that the substrate is recognized by the dimer and the dodecamer equally well. The similar calculated k_{cat} reflects that the active site remains unchanged upon oligomerization. In this case, the size of the substrate is too small to sample the oligomerization state of the aminopeptidase. Thus, in the case of PhTET2, the oligomerization do not affect the active site and catalytic pocket configurations, and has little effect on the recognition and trimming of N-terminal amino acids. However, when studying the catalytic activity of TET dimers and dodecamers as a function of substrate length, we found that the dodecamers are more efficient in hydrolyzing long polypeptide substrates as compared to the dimers. The kinetic parameters indicated that the dodecamer possesses a better efficiency than the dimer toward long substrates: the k_{cat} of the amidohydrolytic reaction, reflecting the catalytic efficiency of the system, is considerably reduced for the free dimer, while the K_m , reflecting the affinity of the active site and the catalytic pocket for the N-terminal amino acid, remains the same between the dimer and the dodecamer. Thus, during the reaction, the same number of peptidase-substrate complexes are formed, but these complexes are more productive in the case of the dodecamer. In contrast, the peptidase-substrate complexes formed by the dimer are unproductive and are not true Michaelis-Menten complexes and thus, cannot be turned-over. Therefore, in the case of the PhTET complex, the self-compartmentalization provides a way to enhance the enzyme efficiency when the substrate size increase. This represents another type of peptidase functional regulation driven by self-oligomerization. The interior of the TET peptidases consist in four polypeptide navigation channels that cross the particles from the entry pores situated on the facets of the tetrahedrons toward the catalytic chambers located within each apex (19,28). A model for polypeptide processing was proposed based on the structural and enzymatic comparisons of the three TET enzymes from *P. horikoshii*. In this model, a series of mobile loops and electrostatic attractions/repulsions in the entry channels and in the catalytic chambers would orient the N-terminus of the polypeptides toward the negatively charged active sites (19,28). In unassembled TET dimers the polypeptide

navigation system is not present. This would explain why the TET dimer is disabled to break down long polypeptides.

P. horikoshii is a hyperthermophilic microorganism that grows optimally at 95°C (54). In this work, it has also been shown that, *in vitro*, the free dimers are as stable at physiological extreme temperatures as the assembled TET particles, with half-lives of several hours at 80°C. Different strategies are adopted by thermozymes to stabilize their native conformation at extreme temperatures (55). Among these, oligomerization has been proposed to represent an important determinant (56). In the case of the TET system, our results show that the dodecameric quaternary structure has little role in the high thermal stability of the enzyme. In fact, the monomer-monomer interfaces in the TET dimer consist of extended networks of ionic bonds that are likely to contribute to the high thermal stability of the enzyme as a free dimer. Therefore, dimers can be accumulated as stable precursors of the TET dodecamers *in vivo*.

There is little information available about the *in vivo* oligomeric states of large energy-independent peptidase complexes. We showed here that the PhTET2 dimer co-exists with the dodecamer in cellular extracts. A similar observation was also made under hypersaline conditions in the extreme halophilic archaeon *H. salinarium*. Unlike *Pyrococcus*, the *Halobacterium* genome contains only one copy of TET peptidase. Thus, it is reasonable to propose that the dimer-dodecamer equilibrium is a hallmark for TET peptidases and that a specific regulation occurs *in vivo* to control the oligomerization state of TET. Since oligomerization affects PhTET2 activity with respect to the size of the polypeptidic substrates, a regulated oligomerization would therefore allow the TET particle to process a broad variety of peptides, from dipeptides to long polypeptides, in response to varying physiological demands: while the TET dimer would act preferentially on small peptides for energetic and anabolic purposes, its assembly into dodecamers and the concomitant formation of the polypeptide navigation system would trigger the intracellular aminopeptidase activity toward longer peptides such as those produced by the 20S proteasome or toward peptides possessing specific biological activities. Thus, the control of the amount of assembled TET *in vivo* may represent an important regulatory step in protein degradation and in many specific

biological functions based on polypeptide activity. Regarding that, *in vitro*, the TET oligomerization appears to be a rapid process, and given that the assembled TET particles are extremely robust, it is likely that the *in vivo* regulatory mechanisms involve the stabilization

of the dimeric species. Studies are in progress in our laboratory to identify this mechanism.

REFERENCES

1. Varshavsky, A. (2005) Regulated protein degradation. *Trends in biochemical sciences* **30**, 283-286
2. Goldberg, A. L. (2003) Protein degradation and protection against misfolded or damaged proteins. *Nature* **426**, 895-899
3. Saric, T., Graef, C. I., and Goldberg, A. L. (2004) Pathway for degradation of peptides generated by proteasomes: a key role for thimet oligopeptidase and other metallopeptidases. *J Biol Chem* **279**, 46723-46732
4. Gonzales, T., and Robert-Baudouy, J. (1996) Bacterial aminopeptidases: properties and functions. *FEMS Microbiol Rev* **18**, 319-344
5. Taylor, A. (1993) Aminopeptidases: towards a mechanism of action. *Trends Biochem Sci* **18**, 167-171
6. Tasaki, T., Sriram, S. M., Park, K. S., and Kwon, Y. T. (2012) The N-End Rule Pathway. *Annu Rev Biochem*
7. van Endert, P. (2011) Post-proteasomal and proteasome-independent generation of MHC class I ligands. *Cellular and molecular life sciences : CMLS* **68**, 1553-1567
8. Matsui, M., Fowler, J. H., and Walling, L. L. (2006) Leucine aminopeptidases: diversity in structure and function. *Biol Chem* **387**, 1535-1544
9. Guzman-Rojas, L., Rangel, R., Salameh, A., Edwards, J. K., Dondossola, E., Kim, Y. G., Saghatelian, A., Giordano, R. J., Kolonin, M. G., Staquicini, F. I., Koivunen, E., Sidman, R. L., Arap, W., and Pasqualini, R. (2012) Cooperative effects of aminopeptidase N (CD13) expressed by nonmalignant and cancer cells within the tumor microenvironment. *Proc Natl Acad Sci U S A* **109**, 1637-1642
10. Holz, R. C., Bzymek, K. P., and Swierczek, S. I. (2003) Co-catalytic metallopeptidases as pharmaceutical targets. *Curr Opin Chem Biol* **7**, 197-206
11. Geier, E., Pfeifer, G., Wilm, M., Lucchiari-Hartz, M., Baumeister, W., Eichmann, K., and Niedermann, G. (1999) A giant protease with potential to substitute for some functions of the proteasome. *Science* **283**, 978-981.
12. Remaut, H., Bompard-Gilles, C., Goffin, C., Frere, J. M., and Van Beeumen, J. (2001) Structure of the *Bacillus subtilis* D-aminopeptidase DppA reveals a novel self-compartmentalizing protease. *Nat Struct Biol* **8**, 674-678
13. Burley, S. K., David, P. R., Sweet, R. M., Taylor, A., and Lipscomb, W. N. (1992) Structure determination and refinement of bovine lens leucine aminopeptidase and its complex with bestatin. *J Mol Biol* **224**, 113-140
14. Joshua-Tor, L., Xu, H. E., Johnston, S. A., and Rees, D. C. (1995) Crystal structure of a conserved protease that binds DNA: the bleomycin hydrolase, Gal6. *Science* **269**, 945-950.
15. Tamura, T., Tamura, N., Cejka, Z., Hegerl, R., Lottspeich, F., and Baumeister, W. (1996) Tricorn protease--the core of a modular proteolytic system. *Science* **274**, 1385-1389

16. Du, X., Choi, I. G., Kim, R., Wang, W., Jancarik, J., Yokota, H., and Kim, S. H. (2000) Crystal structure of an intracellular protease from *Pyrococcus horikoshii* at 2-Å resolution. *Proc Natl Acad Sci U S A* **97**, 14079-14084
17. Delfosse, V., Girard, E., Birck, C., Delmarcelle, M., Delarue, M., Poch, O., Schultz, P., and Mayer, C. (2009) Structure of the archaeal pab87 peptidase reveals a novel self-compartmentalizing protease family. *PLoS one* **4**, e4712
18. Franzetti, B., Schoehn, G., Hernandez, J. F., Jaquinod, M., Ruigrok, R. W., and Zaccari, G. (2002) Tetrahedral aminopeptidase: a novel large protease complex from archaea. *The EMBO journal* **21**, 2132-2138
19. Schoehn, G., Vellieux, F. M., Asuncion Dura, M., Receveur-Brechot, V., Fabry, C. M., Ruigrok, R. W., Ebel, C., Roussel, A., and Franzetti, B. (2006) An archaeal peptidase assembles into two different quaternary structures: A tetrahedron and a giant octahedron. *The Journal of biological chemistry* **281**, 36327-36337
20. Talon, R., Kahn, R., Dura, M. A., Maury, O., Vellieux, F. M., Franzetti, B., and Girard, E. (2011) Using lanthanoid complexes to phase large macromolecular assemblies. *Journal of synchrotron radiation* **18**, 74-78
21. Rawlings, N. D., Barrett, A. J., and Bateman, A. (2012) MEROPS: the database of proteolytic enzymes, their substrates and inhibitors. *Nucleic Acids Res* **40**, D343-350
22. Russo, S., and Baumann, U. (2004) Crystal structure of a dodecameric tetrahedral-shaped aminopeptidase. *The Journal of biological chemistry* **279**, 51275-51281
23. Borissenko, L., and Groll, M. (2005) Crystal structure of TET protease reveals complementary protein degradation pathways in prokaryotes. *Journal of molecular biology* **346**, 1207-1219
24. Kim, D., San, B. H., Moh, S. H., Park, H., Kim, D. Y., Lee, S., and Kim, K. K. (2010) Structural basis for the substrate specificity of PepA from *Streptococcus pneumoniae*, a dodecameric tetrahedral protease. *Biochemical and biophysical research communications* **391**, 431-436
25. Chen, Y., Farquhar, E. R., Chance, M. R., Palczewski, K., and Kiser, P. D. (2012) Insights into substrate specificity and metal activation of mammalian tetrahedral aspartyl aminopeptidase. *The Journal of biological chemistry* **287**, 13356-13370
26. Chaikuad, A., Pilka, E. S., Riso, A. D., Delft, F. V., Kavanagh, K. L., Venien-Bryan, C., Oppermann, U., and Yue, W. W. (2012) Structure of human aspartyl aminopeptidase complexed with substrate analogue: insight into catalytic mechanism, substrate specificity and M18 peptidase family. *BMC Struct Biol* **12**, 14
27. Dura, M. A., Receveur-Brechot, V., Andrieu, J. P., Ebel, C., Schoehn, G., Roussel, A., and Franzetti, B. (2005) Characterization of a TET-like aminopeptidase complex from the hyperthermophilic archaeon *Pyrococcus horikoshii*. *Biochemistry* **44**, 3477-3486
28. Dura, M. A., Rosenbaum, E., Larabi, A., Gabel, F., Vellieux, F. M., and Franzetti, B. (2009) The structural and biochemical characterizations of a novel TET peptidase complex from *Pyrococcus horikoshii* reveal an integrated peptide degradation system in hyperthermophilic Archaea. *Molecular microbiology* **72**, 26-40
29. Rosenbaum, E., Ferruit, M., Dura, M. A., and Franzetti, B. (2011) Studies on the parameters controlling the stability of the TET peptidase superstructure from *Pyrococcus horikoshii* revealed a crucial role of pH and catalytic metals in the oligomerization process. *Biochimica et biophysica acta* **1814**, 1289-1294
30. Ando, S., Ishikawa, K., Ishida, H., Kawarabayasi, Y., Kikuchi, H., and Kosugi, Y. (1999) Thermostable aminopeptidase from *Pyrococcus horikoshii*. *FEBS letters* **447**, 25-28

31. Chevrier, B., Schalk, C., D'Orchymont, H., Rondeau, J. M., Moras, D., and Tarnus, C. (1994) Crystal structure of *Aeromonas proteolytica* aminopeptidase: a prototypical member of the co-catalytic zinc enzyme family. *Structure* **2**, 283-291
32. Godfroy, A., Raven, N. D., and Sharp, R. J. (2000) Physiology and continuous culture of the hyperthermophilic deep-sea vent archaeon *Pyrococcus abyssi* ST549. *FEMS Microbiol Lett* **186**, 127-132
33. Chamieh, H., Guetta, D., and Franzetti, B. (2008) The two PAN ATPases from *Halobacterium* display N-terminal heterogeneity and form labile complexes with the 20S proteasome. *The Biochemical journal* **411**, 387-397
34. Schuck, P. (2000) Size-distribution analysis of macromolecules by sedimentation velocity ultracentrifugation and lamm equation modeling. *Biophys J* **78**, 1606-1619
35. Svergun, D. I., Petoukhov, M. V., and Koch, M. H. (2001) Determination of domain structure of proteins from X-ray solution scattering. *Biophysical journal* **80**, 2946-2953
36. Volkov, V. V., and Svergun, D. I. (2003) Uniqueness of ab initio shape determination in small-angle scattering. *J Appl Crystallogr* **36**, 860-864
37. Wriggers, W. (2010) Using Situs for the integration of multi-resolution structures. *Biophysical reviews* **2**, 21-27
38. Chacon, P., and Wriggers, W. (2002) Multi-resolution contour-based fitting of macromolecular structures. *J Mol Biol* **317**, 375-384
39. Svergun, D., Barberato, C., and Koch, M. H. J. (1995) CRY SOL - A program to evaluate x-ray solution scattering of biological macromolecules from atomic coordinates. *J Appl Crystallogr* **28**, 768-773
40. Emsley, P., Lohkamp, B., Scott, W. G., and Cowtan, K. (2010) Features and development of Coot. *Acta crystallographica. Section D, Biological crystallography* **66**, 486-501
41. Frank, J., Radermacher, M., Penczek, P., Zhu, J., Li, Y., Ladjadj, M., and Leith, A. (1996) SPIDER and WEB: processing and visualization of images in 3D electron microscopy and related fields. *Journal of structural biology* **116**, 190-199
42. Frottin, F., Martinez, A., Peynot, P., Mitra, S., Holz, R. C., Giglione, C., and Meinnel, T. (2006) The proteomics of N-terminal methionine cleavage. *Mol Cell Proteomics* **5**, 2336-2349
43. Ginzburg, M., Sachs, L., and Ginzburg, B. Z. (1970) Ion metabolism in a *Halobacterium*. I. Influence of age of culture on intracellular concentrations. *J Gen Physiol* **55**, 187-207.
44. Lindner, P., and Zemb, T. (2002) *Neutrons, X-rays and Light: Scattering Methods Applied to Soft Condensed Matter*. Elsevier ed.,
45. Svedberg, T., Bauer, J. H., and Pedersen, K. O. (1940) *The ultracentrifuge*, Clarendon Press, Oxford
46. Lupas, A., Flanagan, J. M., Tamura, T., and Baumeister, W. (1997) Self-compartmentalizing proteases. *Trends Biochem Sci* **22**, 399-404.
47. Groll, M., Ditzel, L., Lowe, J., Stock, D., Bochtler, M., Bartunik, H. D., and Huber, R. (1997) Structure of 20S proteasome from yeast at 2.4 Å resolution. *Nature* **386**, 463-471
48. Brandstetter, H., Kim, J. S., Groll, M., and Huber, R. (2001) Crystal structure of the tricorn protease reveals a protein disassembly line. *Nature* **414**, 466-470
49. O'Farrell, P. A., Gonzalez, F., Zheng, W., Johnston, S. A., and Joshua-Tor, L. (1999) Crystal structure of human bleomycin hydrolase, a self-compartmentalizing cysteine protease. *Structure* **7**, 619-627

50. Thompson, M. W., Miller, J., Maurizi, M. R., and Kempner, E. (1998) Importance of heptameric ring integrity for activity of Escherichia coli ClpP. *Eur J Biochem* **258**, 923-928
51. Burley, S. K., David, P. R., Taylor, A., and Lipscomb, W. N. (1990) Molecular structure of leucine aminopeptidase at 2.7-Å resolution. *Proc Natl Acad Sci U S A* **87**, 6878-6882
52. Marquardt, U., Zettl, F., Huber, R., Bode, W., and Sommerhoff, C. (2002) The crystal structure of human alpha1-tryptase reveals a blocked substrate-binding region. *Journal of molecular biology* **321**, 491-502
53. Debela, M., Magdolen, V., Grimminger, V., Sommerhoff, C., Messerschmidt, A., Huber, R., Friedrich, R., Bode, W., and Goettig, P. (2006) Crystal structures of human tissue kallikrein 4: activity modulation by a specific zinc binding site. *Journal of molecular biology* **362**, 1094-1107
54. Gonzalez, J. M., Masuchi, Y., Robb, F. T., Ammerman, J. W., Maeder, D. L., Yanagibayashi, M., Tamaoka, J., and Kato, C. (1998) *Pyrococcus horikoshii* sp. nov., a hyperthermophilic archaeon isolated from a hydrothermal vent at the Okinawa Trough. *Extremophiles* **2**, 123-130
55. Jaenicke, R., and Bohm, G. (1998) The stability of proteins in extreme environments. *Curr Opin Struct Biol* **8**, 738-748
56. Clantin, B., Tricot, C., Lonhienne, T., Stalon, V., and Villeret, V. (2001) Probing the role of oligomerization in the high thermal stability of *Pyrococcus furiosus* ornithine carbamoyltransferase by site-specific mutants. *Eur J Biochem* **268**, 3937-3942

Acknowledgments – We acknowledge financial supports from the Agence Nationale de la Recherche (Grants "MacroTET"-BLAN-07-3 204002 and "Archelyse" ANR-12-BSV8-0019-01) and the GRD Ecchis. A.A. was supported by a PhD scholarship from the French Ministry for Research and Technology. M.A.D and M.C were supported by a French National Research Agency post-doctoral fellowship. We thank J. Le Bars for help in *P.horikoshii* cultivation. We thank A. Le Roy and C. Ebel, from the PSB/IBS platform for the assistance and access to the instrument of Analytical Ultracentrifugation. We thank D. Fenel and C. Moriscot from the PSB/IBS for the Electron Microscopy.

FIGURE LEGENDS

FIGURE 1. Purification of a PhTET2 dimeric complex. A. Native gel electrophoresis analysis of the PhTET2 protein that was obtained after expression of the recombinant wild type and the pentamutant (R217S, R220S, F224S, H248S, I292A) proteins in *E. coli*, heat shock clarification and separation by Resource Q ion exchange chromatography. Wt is the purified wild-type PhTET2 dodecamer, Pool A corresponds to a low molecular weight complex, while the major constituent of Pool B is a high molecular weight complex that migrates as the wild-type PhTET2 dodecamer. B. Superpose 6 column chromatography purification of dimeric and dodecameric mutant PhTET2 complexes. The A₂₈₀ absorption profiles are presented together with negative staining electron microscopy images taken from aliquots of the pooled peak fractions. The elution volume and the shape of the purified complexes from Pool A and Pool B correspond to dimers and TET dodecamers, respectively. This information was further confirmed by AUC (Fig. 5) and SAXS (Figs. 3 and 4).

FIGURE 2. Determination of TET oligomerization states in *Pyrococcus horikoshii* and *Halobacterium salinarum* cells. A. Immunodetection of the natives TET2 complexes from *Pyrococcus horikoshii* (Ph). Post-membrane extracts (S30) were loaded on a 5-25% sucrose density gradient and resolved by ultracentrifugation. The fraction numbers are indicated on top and the arrow represents the sedimentation orientation. The proteins from each fraction were separated on a 12% SDS-PAGE gel and the presence of the PhTET2 protein was revealed by Western blot by using specific antibodies.

Two panels below: Coomassie blue staining of 12% SDS-PAGE gels. In this experiment, purified dimeric and dodecameric PhTET2 complexes were resolved on sucrose gradient by using the same protocol as for the S30 extracts. These complexes were obtained from a mutant protein in which aminoacids have been changed in order to slow down the particle assembling process (see Fig. 1). The positions of the dimer and the dodecamer in the gradients are indicated and correspond to the immunodetected PhTET2 complexes in the cell extracts. B. Immunodetection of the native TET complexes from the extreme halophilic strain *Halobacterium salinarum* (Hs). S30 extracts were fractionated in native hypersaline conditions on a 5-20% sucrose gradient. The gradient was calibrated with halophilic protein complexes of known molecular sizes (indicated above) as described in Chamieh *et al*, 2008. A low molecular weight TET complex co-exists with the assembled TET dodecamer in the cytosols of Ph and Hs.

FIGURE 3. Small angle X-ray scattering (SAXS) study of the PhTET2 mutant and wild type dodecamers. SAXS curves from both particles superpose very well over the whole angular range studied, indicating that the quaternary arrangements of both particles are identical in solution. The back-calculated SAXS curves (using CRY SOL) from the 12s PhTET2 crystal structure without and with missing fragments (internal loop and N-ter) are also shown.

FIGURE 4. Low-resolution structure of the free PhTET2 dimer. A. Experimental SAXS curves for the mutated PhTET2 dimer in solution. The back-calculated SAXS curves (using CRY SOL) from the 2s PhTET2 with and without missing fragments (internal loop and N-ter) as well as the back-calculated SAXS curves from a V-shaped tetramer and a triangular hexamer are also shown. The experimental SAXS curve superposes well with the back-calculated one from the 2s particle (including the missing loop and the N-ter), indicating that the quaternary arrangements of both particles are very similar in solution. B. Overlay of the final averaged *ab initio* shape reconstruction of the mutated PhTET2 dimer derived from SAXS experiments (grey envelope) with the structure of the PhTET2 dimer inside the TET dodecamer crystallographic model (PDB entry 1Y0R, purple).

FIGURE 5. Biophysical characterization of the PhTET2 assembling pathway. A. Native gel electrophoresis experiment revealing the existence of various intermediate TET oligomeric species after incubation of the purified PhTET2 dimer at different times of incubation, at 4°C, in 50 mM HEPES pH 7.5, 300 mM NaCl. B. Analysis of a sample of purified mutant PhTET2 dimer by analytical ultracentrifugation 7 days after purification. The sample loading concentration was 0.4 mg/ml. Sedimentation coefficients are expressed in Svedberg: 1 S=10⁻¹³ s. Three major species are detected at 4.70, 6.78 and 9.29 S, and two other peaks are visible around 11.91 S and 15.75 S. C. Theoretical sedimentation coefficients for putative PhTET2 assembly intermediates calculated for two different frictional ratios and experimental sedimentation coefficients and respective relative concentration for species detected in the sample analyzed by AUC. The experimental sedimentation coefficients were calculated with the program Sedfit using a continuous c(s) distribution model. Only intermediate forms with even subunit numbers were detected thus indicating that the TET oligomerisation is a non-random controlled process. The tetrameric and hexameric forms are found to be the most abundant in the analyzed sample.

FIGURE 6. Comparison between the different oligomeric models of PhTET2 and the negative staining electron microscopy images. The atomic resolution structure of the different PhTET2 assembling intermediates plus the real dodecameric assembly are represented on the left. For each of these particles a 20 Å resolution three dimensional structure has been calculated. Some typical views obtained by negative staining electron microscopy (lower row) and the three dimensional corresponding isosurface view (top row) are shown for each category. The dimensions of the negative staining squared images are 34 nm x 34 nm whereas the 3D models images are 20 nm x 20 nm

TABLE I. Kinetics constant of mutated PhTET2 dimer and dodecamer against a short (Leu-pNA) and a 11 residues (Met-Lys-Bradikinin) peptide. The k_{cat} is the catalytic efficiency of the enzyme, the K_m is

the Michaelis constant of the enzyme reflecting the affinity of the enzyme for its substrate. The catalytic efficiency of the dimer on a long peptide is lower than the one of the dodecamer. The dodecameric form of PhTET2 is more efficient at processing long peptides than the dimeric form.

FIGURE 7. Time course of hydrolysis of Met-Lys-Bradikinin by the dodecameric and dimeric forms of the PhTET2 pentamutant. Concentration evolution of oxidized o-dianisidine in the reaction mixture as a function of time. For each free amino acid released in solution, one molecule of o-dianisidine is oxidized (see “Materials and Methods”). Because PhTET2 displays very low activity toward basic residues such as Lys, the concentration evolution of oxidized o-dianisidine in solution reflects the activity of PhTET2 only on the full length 11-amino acid substrate peptide. The corresponding kinetics constants are presented in Table I.

FIGURE 8. Oligomerization model of the dodecameric TET particles based on the results obtained by the combination of site-directed mutagenesis, SAXS, AUC, electron microscopy and structural analysis described in this paper. The dimer constitutes the building block and self-assembles into a closed hexamer which involves the association of three dimers (red, magenta and blue). Two open 'mirror' conformations of this complex are in equilibrium and finally associate to form the super-stable dodecameric particle.

Table I. Kinetics constant of mutated PhTET2 dimer and dodecamer against a short (Leu-pNA) and a 11 residues (Met-Lys-Bradikinin) peptide.

		Dodecamer	Dimer
Leu-pNA	k_{cat} (s^{-1})	511 ± 45.9	421.5 ± 33.6
	K_M (mM)	1 ± 0.1	1.1 ± 0.09
	k_{cat}/K_M ($mM^{-1}s^{-1}$)	511 ± 97.09	383.2 ± 61.7
Met-Lys-Bradikinin	k_{cat} (s^{-1})	144.5 ± 9.4	1.5 ± 0.13
	K_M (mM)	1.9 ± 0.114	2 ± 0.07
	k_{cat}/K_M ($mM^{-1}s^{-1}$)	76.05 ± 9.5	0.55 ± 0.06

Figure 1. Purification of a PhTET2 dimeric complex.

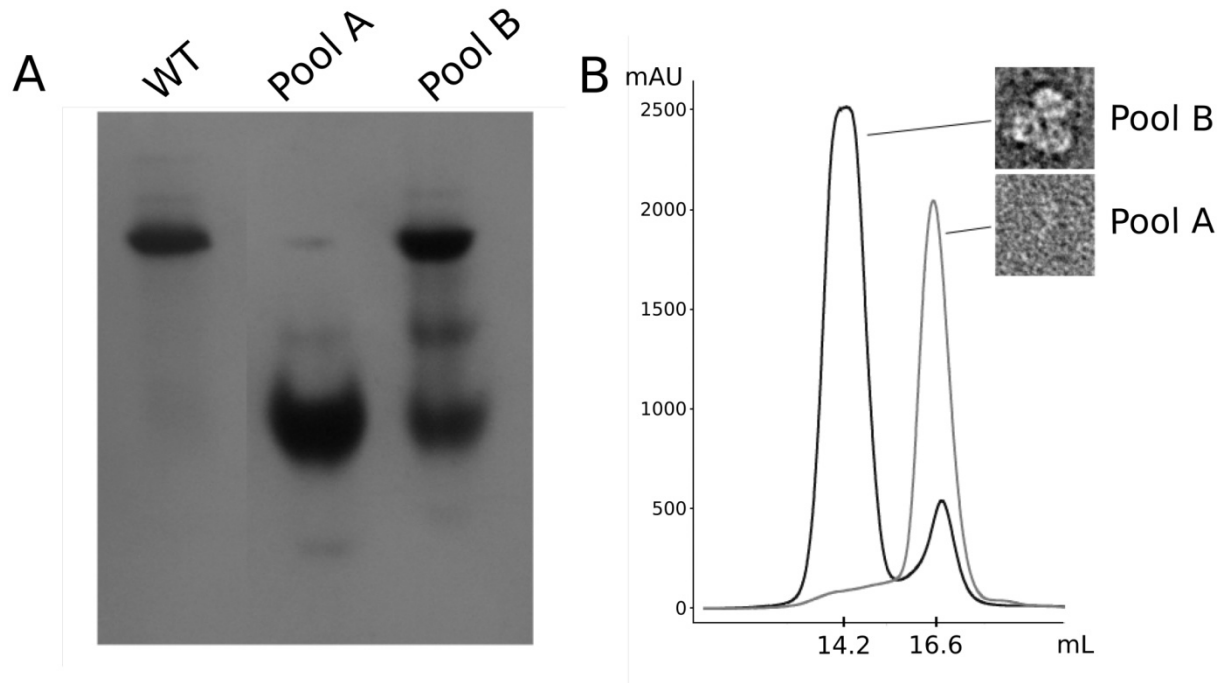


Figure 2. Detemination of TET oligomerization states in *Pyrococcus horikoshii* and *Halobacterium salinarum* cells

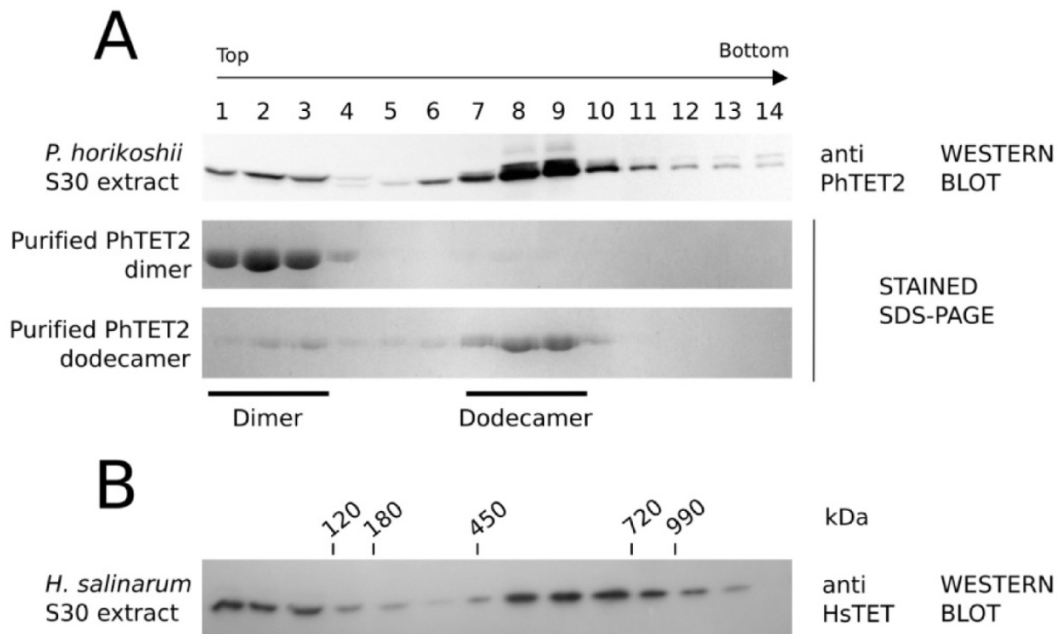


Figure 3. Small angle X-ray scattering (SAXS) study of the PhTET2 mutant and wild type dodecamers.

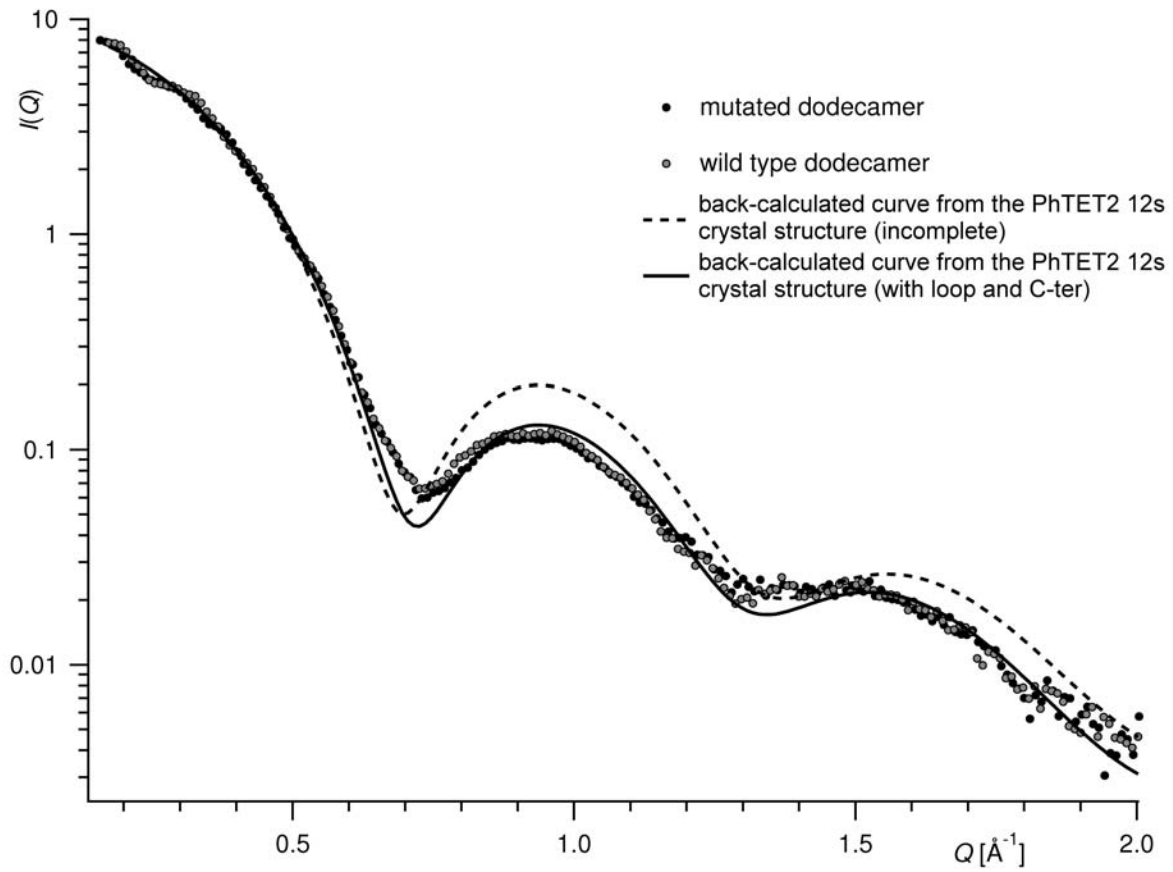


Figure 4. Low-resolution structure of the free PhTET2 dimer.

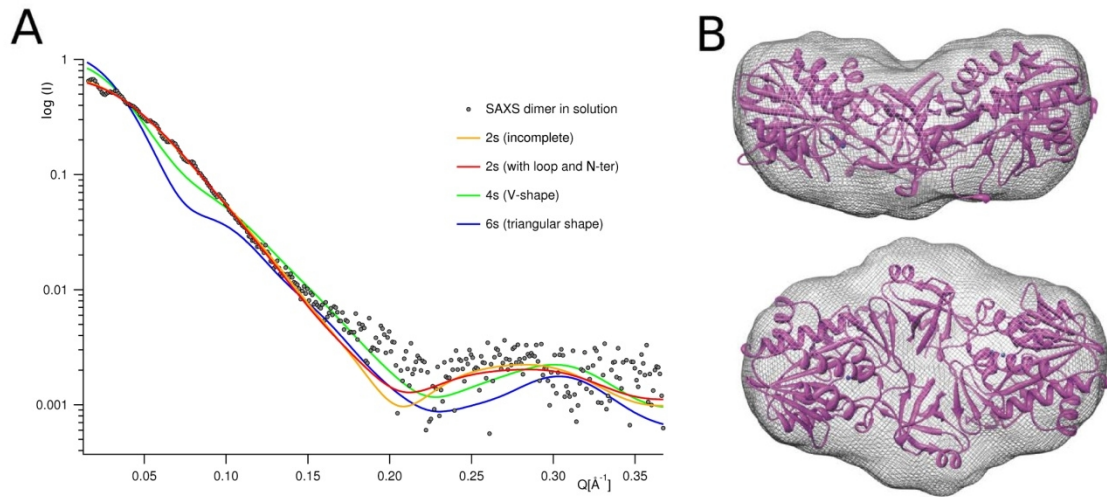


Figure 5 : Biophysical characterization of the PhTET2 assembling pathway.

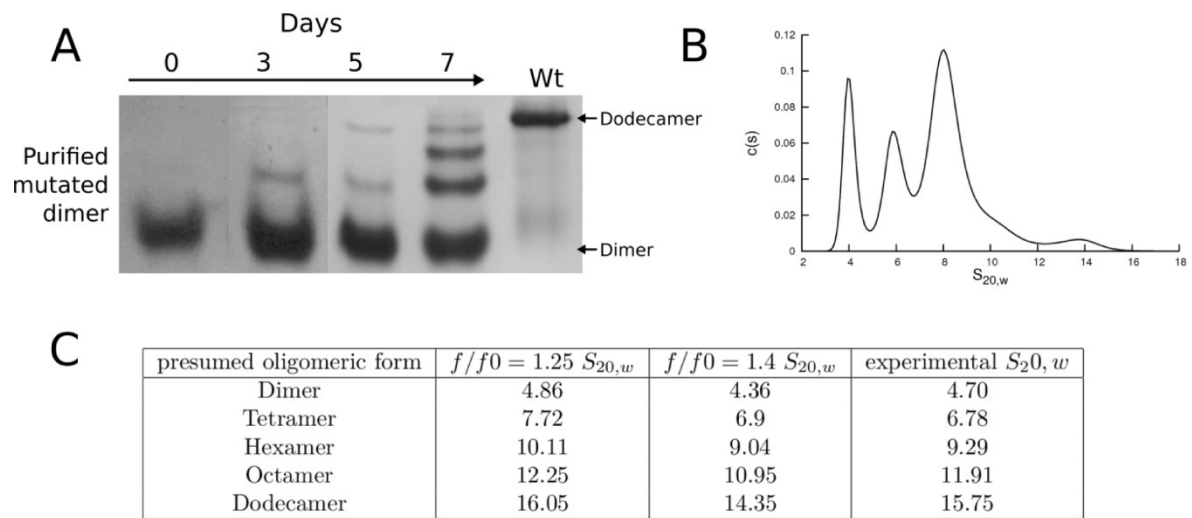


Figure 6. Electron microscopy images compare to low-resolution envelopes of PhTET2 oligomerization intermediates

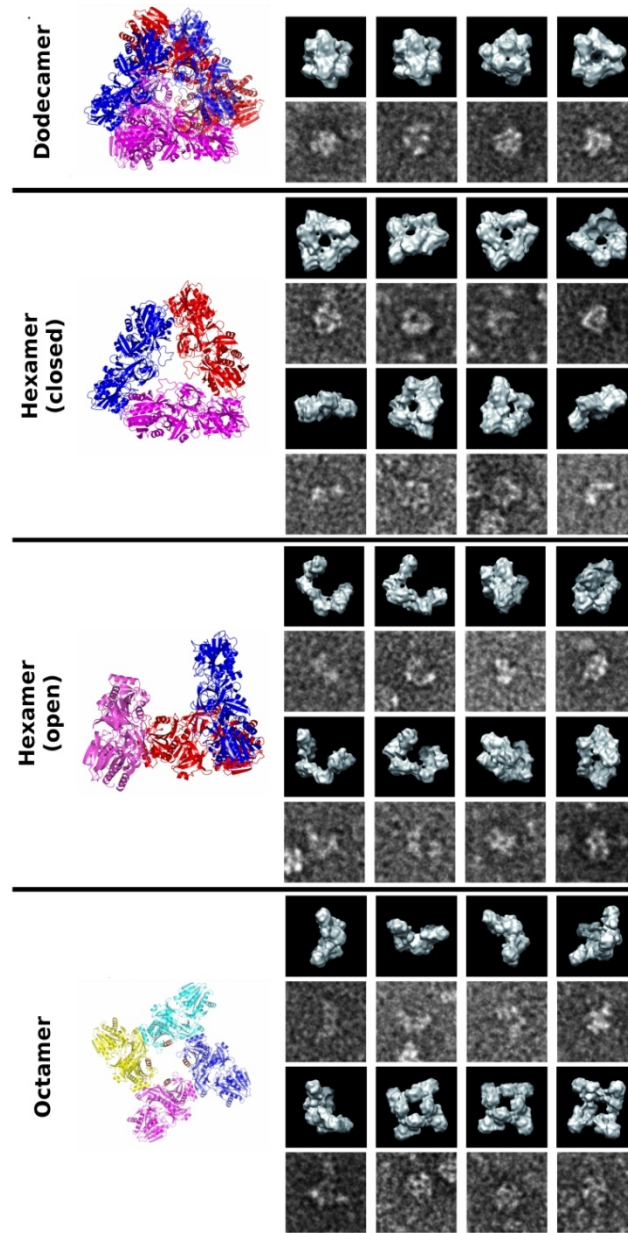


Figure 7. Time course of hydrolysis of Met-Lys-Bradikinin by the dodecameric and dimeric forms of the PhTET2 pentamutant.

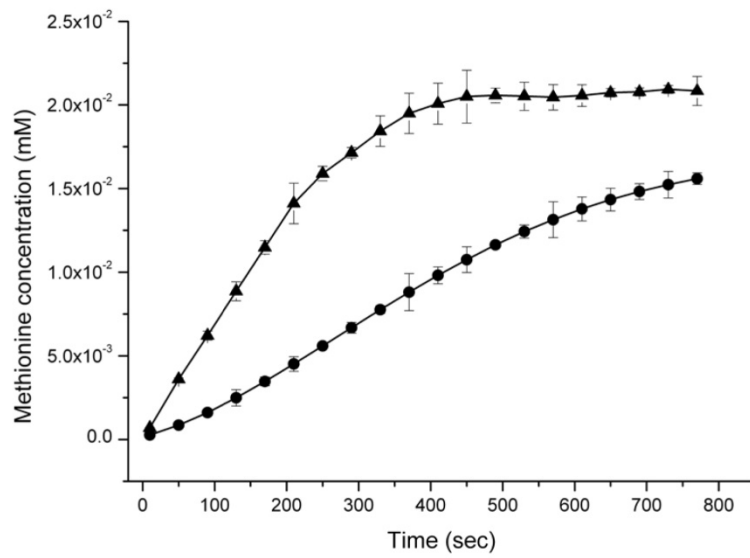
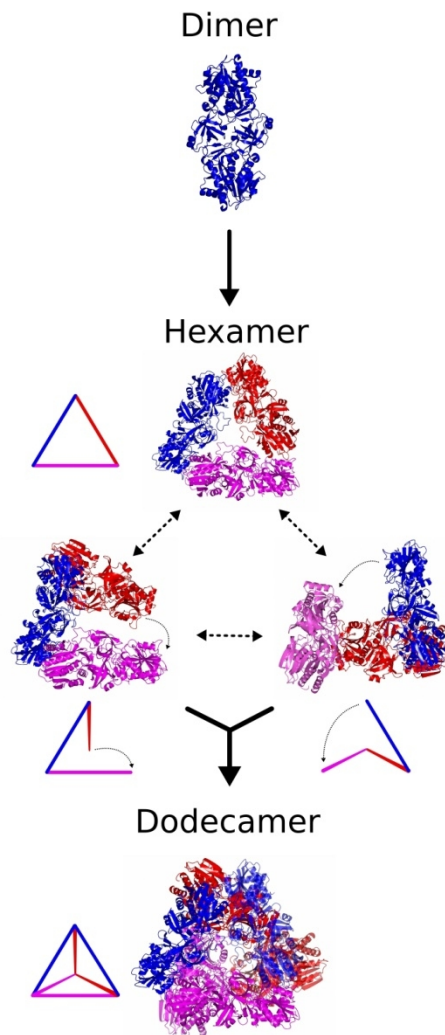


Figure 8. Proposed model for TET oligomerisation.

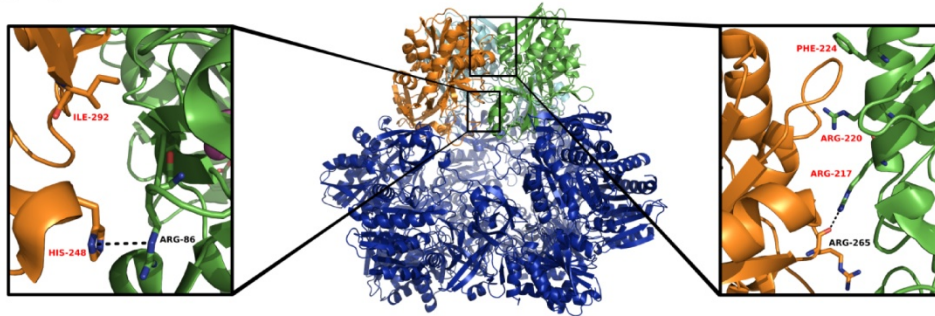


Supplementary Material

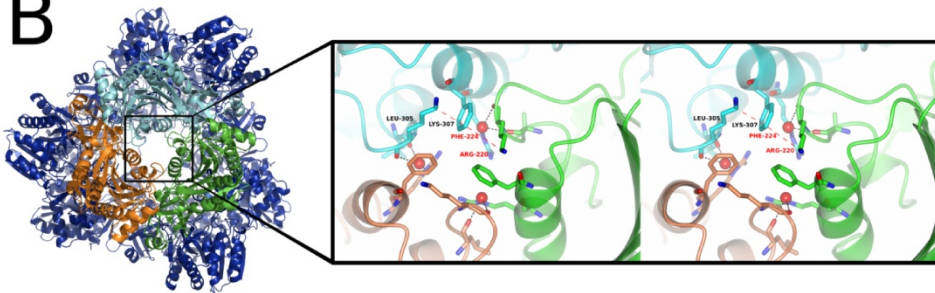
SUPPLEMENTARY FIGURE 1. Positions of PhTET2 mutations and destabilized interfaces. Mutated residues are labelled in red, non-mutated interacting residues are labeled in black. A. Centre: Facet of the tetrahedral PhTET2 particle (PDB entry 1Y0R), three monomers forming one of the apices are coloured. Right: Close-up on the mutated apex interface; the mutations R217S, R220S and F224S are represented. Left: Close-up on the second mutated interface, the mutations H248S and I292A are represented. B. Right: View from one of the apex of the tetrahedron; three monomers forming the apex are coloured. Left: Close-up on the apex interface; residues of the blue monomer are labelled. C. Mutated residues and the corresponding eliminated interactions in the PhTET2 pentamutant. The destabilization of the oligomerisation interface is obtained by the elimination of hydrophobic and polar interactions.

Supplementary Figure 1: Positions of PhTET2 mutations and destabilised interfaces.

A



B



C

Mutation	Interaction type	Amino acid residue implicated	Description	Observations
R217S	Polar	R265	Main chain carbonyl oxygen	Water mediated
		D264	Main chain carbonyl oxygen	
	Hydrophobic	L305	Side chain	Mutation was done to S instead of A to completely avoid this interaction
R220S	Polar	L305	Main chain carbonyl oxygen	Water mediated
		K307	Main chain carbonyl oxygen	Water mediated
		F224S	F224 aromatic ring with side chain	Water mediated
H248S	Polar	E80	Carboxyl group	Water mediated
	Hydrophobic	H78	Side chain	
I292A	Hydrophobic	R86		Side chain
		T77		
		I158		
		A88		